



22nd IAHR International Symposium on Ice

Singapore, August 11 to 15, 2014

Validation of sea ice concentration obtained from the Chinese Marine Satellite (HY-2) microwave radiometer instrument

Lijian Shi^{1*}, Peng Lu², Bin Cheng³, Zhijun Li², Qimao Wang¹, Yunfei Lu¹ and Xiaomin Ye¹

1 National Satellite Ocean Application Service (NSOAS), Beijing, China

2 State Key Laboratory of Coastal and Offshore Engineering, Dalian University of Technology, Dalian, China

3 Finnish Meteorological Institute (FMI), Helsinki, Finland

**shilj@mail.nsoas.gov.cn*

Sea ice concentration (SIC) is one of the most important parameters describing the sea ice characteristics over polar region and a crucial input parameter for various regional numerical weather prediction (NWP) and climate models. Satellite-borne microwave radiometer is the most effective and consistent tool to measure the sea ice concentration over Polar Regions. SIC retrieval method with the brightness temperatures (Tb) from the Chinese marine satellite HaiYang 2 (HY-2) scanning radiometer has been established. The HY-2 retrieval SIC in the Arctic is in good agreement with two operational products from NSIDC and University of Bremen.

In this study, the validation of above three SIC products are presented. Aerial photography conducted during CHINARE-2012 was also employed to produce Arctic sea ice concentration and then compared with the retrieval of satellite remote sensing after spatial interpolation. HY2/NT is 16% higher than the results of aerial photography at the compact ice regions in the central Arctic where the helicopter flights during CHINARE-2012 was carried out. In contrast, the SSMIS/NT data underestimate the in-situ ice concentrations by 17%. While the SSMIS/ASI data show a nice agreement with the result of in-situ photography, possibly because of its higher spatial resolution of 6.25 km than other satellite data. Six SAR images were finally used for the validation of SIC retrievals HY2/NT, SSMIS/NT and SSMIS/ASI. The RMS errors between HY2/NT and SAR, ranging from 22.42% to 33.15%, are larger than that of SSMIS/NT and SSMIS/ASI which are in the range of 13-34% with an average of 22%. The RMS errors in ice edge areas are higher than that of the interior areas. If pixels at ice edges are removed, the RMS between SAR derived ice concentration and three microwave retrievals falls below 10%.

1. Introduction

Sea ice concentration (SIC) is defined as the fraction of sea ice over a unit area. Ice concentration can be given as a fraction or as a percentage. It is one of the most important parameters describing the sea ice characteristics over polar region. It is also a crucial input parameter for various regional numerical weather prediction (NWP) and climate models. Satellite-borne microwave radiometer is the most effective and consistent tool to measure the sea ice concentration over Polar Regions. NSIDC (National Snow and Ice Data Center) provides a consistent time series of ice concentration over the whole Arctic in the polar stereographic projection with a grid cell size of 25 x 25 km since 1978. This historical data set is retrieved from brightness temperatures of the following sensors: the Nimbus-7 Scanning Multichannel Microwave Radiometer (SMMR), the Defense Meteorological Satellite Program (DMSP) Special Sensor Microwave/Imagers (SSM/I). Sensors currently in orbit, such as DMSP-F17 & 18 Special Sensor Microwave Imager/Sounder (SSMIS) and GCOM-W1 AMSR2, can be used to complement this time series.

Many algorithms have been studied to retrieve the SIC based on the brightness temperature of microwave radiometers. NASA Team (Cavalieri, 1991) and Bootstrap (Comiso, 1995), which are based on the T_b of 19 GHz and 37 GHz, are the most widely used algorithms to derive SIC in 25 km resolution. Since 1992 the 85 GHz channels of SSMI with a higher spatial resolution became available and some corresponding methods were developed such as NASA TEAM2 (Markus and Cavalieri, 2000); ASI (Svendsen et al, 1987) and LOMAX (Lomax et al, 1995). For example, ASI algorithm can be used to provide 6.25 km sea ice concentration products, in which the resolution is doubled compared to the NASA Team algorithm resolution. Among the above methods, NASA TEAM, NASA TEAM2 and LOMAX can also provide the concentration of first-year ice (FYI) and multiyear ice (MYI).

On August 16, 2011, the HY-2 satellite was launched. This is the very first Chinese satellite that designed to monitor the marine dynamic environment. SIC retrieval method with the brightness temperatures (T_b) from the HY-2 scanning radiometer has been established. This paper focuses the validation of validation of SIC product with aerial photography during CHINARE-2012 and the SAR wind speed imagery.

2. Data

2.1 SIC data

To attain comprehensive observations on the marine dynamic environment, the HY-2 satellite is equipped with four microwave remote sensors: radar altimeter, microwave scatterometer, scanning microwave radiometer and calibration microwave radiometer. Scanning microwave radiometer measures at frequencies of 6.6, 10.7, 18.7, 23.8 and 37.0GHz, respectively. In addition to the band of 23.8 GHz with vertical polarization, the other four bands operate with horizontal and vertical polarization. The scanning swath of the radiometer is 1600 km. The sensitivity of 37.0GHz band is better than 0.8 K and that of other bands is better than 0.5 K. Using this sensor, many marine environmental parameters such as sea surface temperature, sea

surface wind field, atmospheric water vapor, cloud water content, SIC and precipitation, can be inverted. The brightness temperature data of HY-2 during CHINARE-2012 and in Nov. 2013 were used to get the corresponding SIC. These retrieved SIC data from HY-2 are denoted by HY2/NT thereafter.

Two operational SIC products were accessed for this study. One is provided by NSIDC with SSMIS data of DMSP F17 by the NASA TEAM algorithm (Cavalieri et al., 1996), denoted by SSMIS/NT thereafter. The spatial resolution is 25 km and its grid position is the same with that of HY-2 microwave radiometer Level 3 data. Another is from University of Bremen with SSMIS data of DMSP F18 and the ASI algorithm is used for retrieval, denoted by SSMIS/ASI thereafter. The resolution of the ASI product is 6.25 km and it is used after interpolating into 25 km grids.

2.2 Aerial photography of Arctic sea ice during CHINARE-2012

The 5th Chinese National Arctic Research Expedition (CHINARE) was conducted from 2 July until 27 September 2012. The Research Vessel (R/V) Xuelong from the Polar Research Institute of China was used as the expedition platform. The R/V Xuelong firstly travelled through the Northeast Arctic passage and reached Iceland on 16 August and then shipped back to the Bering Sea through higher latitude routes. Along the cruise track, different kinds of instruments had been employed to observe the sea ice encountered by the ship, such as EM-31, ice buoy, radiometer, photography, etc. Among which, three helicopter flights were conducted to perform an aerial survey of sea ice conditions when the R/V Xuelong close to the central Arctic on its way back to the PAS. The flight routes and ship tracks are shown in Fig. 1. To conduct the aerial surveys, an iron box was mounted outside the helicopter in a downward-facing orientation. The box contained a Canon G9 camera, a portable GPS, and a pressure differential altimeter. The camera worked with a resolution of 4000×3000 pixels. The flight altitude varied according to weather conditions, but was generally around 300 m. At this height, each snap shot covered an area of approximately $128 \text{ m} \times 96 \text{ m}$, yielding a resolution of 0.03 m per pixel. The images were spaced without overlapping, and each image represented an independent scene. The total time for all flights was 184 minutes, and 1444 images were collected. Only 2% of images could not be processed because of the poor contrast resulting from low clouds or fog. The images covered the locations 84.3°N – 86.7°N and 119.8°E – 154.1°E .

During the flight surveys, sea ice was undergoing a transition period from the late melting phase to the early freeze-up phase. Snow-covered ice, melt pond and open lead are the three obvious components on the Arctic Ocean surface. Processing of these aerial images is exactly consistent with that for previous CHINAREs. After an image was partitioned into three-category surface fractions through manually selecting red, green, and blue (RGB) thresholds based on color distribution histograms (Perovich et al., 2002; Inoue et al., 2008), the snow/ice, open leads and melt ponds can be then distinguished from the images. SIC is defined as the sum of the aerial fractions of snow/ice and melt ponds.

2.3 SAR wind speed image

U. S. National Ice Center (NIC) distributes the operational wind speed product over mid and high latitudes of Arctic derived from synthetic aperture radar (SAR) imagery. The product is a

RGB image in geotiff format and WGS-84 datum. The ice-covered area can be easily segmented from the open ocean area in these images. Each image is with 1200×1200 pixels and with 500 m spatial resolution, and the images are supplied free and daily, providing a good choice for the calibration of SIC retrievals from radiometer data except for the initial SAR imagery. Six wind speed images in Nov. 2013 were selected to validate our result, SSMIS/NT and SSMIS/ASI. Figure 1 shows the locations of these images with purple polygons, covering parts of Greenland Sea, Kara Sea and Chukchi Sea, respectively.

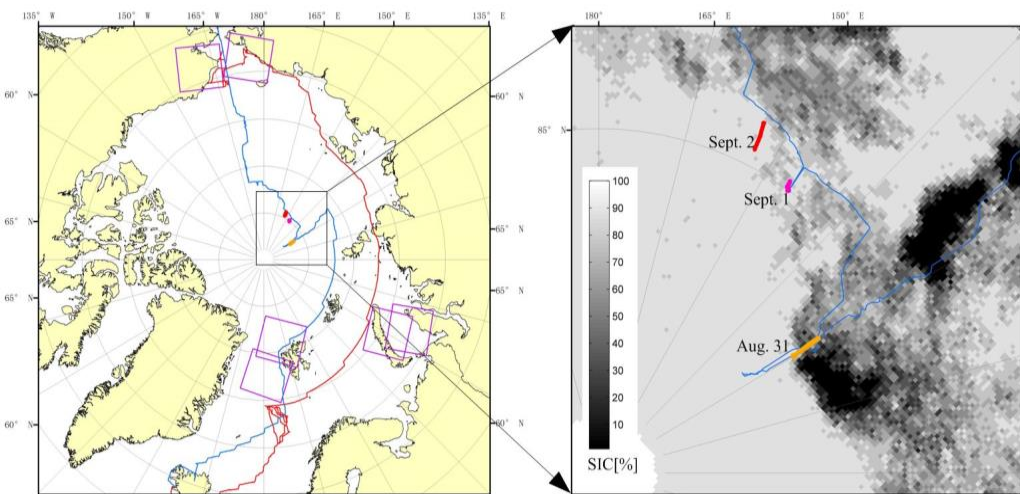


Figure 1. Cruise tracks (red line for the outward journey and blue for the backward journey) of R/V Xuelong during CHINARE-2012 and coverage of 6 SAR wind speed images (purple rectangle) on the left. Routes of three helicopter flights of aerial photography in the central Arctic (orange, pink and red lines) with overlapping SIC of Aug. 31 2012 from SSMIS/ASI on the right.

3. SIC algorithm

SIC retrieval algorithm with the brightness temperatures (Tb) from the HY-2 scanning radiometer has been established. The two quantities based on brightness temperatures used in the NT algorithm are Polarization Gradient Ratio (PR) and Spectral Gradient Ratio (GR), which are defined as:

$$PR(18.7) = (T_{b,18.7V} - T_{b,18.7H}) / (T_{b,18.7V} + T_{b,18.7H}) \quad [1]$$

$$GR(37/18.7) = (T_{b,37V} - T_{b,18.7V}) / (T_{b,37V} + T_{b,18.7V}) \quad [2]$$

where $T_{b,p}$ is the brightness temperature at a specific frequency for the specific polarized component p (vertical V or horizontal H). These ratios are highly independent on the variations in ice temperature, so the temporal and spatial changes of ice temperature can be eliminated in the SIC retrieval. Then concentrations of FYI and MYI can be expressed by the above ratios as:

$$C_{MYI} = \frac{M_0 + M_1 \cdot PR + M_2 \cdot PR + M_3 \cdot PR \cdot GR}{D} \quad [3]$$

$$C_{FYI} = \frac{F_0 + F_1 \cdot PR + F_2 \cdot GR + F_3 \cdot PR \cdot GR}{D} \quad [4]$$

where $D = D_0 + D_1 \cdot PR + D_2 \cdot GR + D_3 \cdot PR \cdot GR$. The coefficients M_i , F_i and D_i ($i = 0 \sim 3$) are the functions of nine brightness temperature values. These nine brightness temperatures, called tie points, are the observed typical radiance for open water (OW), FYI and MYI conditions for the three channels employed. The values of these nine brightness temperatures are given in Table 1.

Table 1. Selected tie points Tb (K) of 18.7V, 18.7H and 37V for the three surface types.

Surface type	18V	18H	37V
OW	150.2684	101.7104	201.2541
FYI	222.6900	211.2785	247.9931
MYI	208.2987	194.4125	215.8485

The false indication of sea ice over the open ocean or adjacent to the edge of sea ice is a problem in mapping the polar sea ice concentration. There occur spurious concentration results due to presence of atmospheric water vapor, cloud liquid water, precipitation and even rough surface by winds. For an open water temperature of 271 K, typical near the ice edge, the GR(37/19) threshold generally works well in most cases over the polar latitudes, but it fails at the lower latitudes or in summer conditions with water-vapor values greater than 2 cm. This problem can be resolved with GR(22/19) filter which is defined as the Spectral Gradient Ratio of the 22 GHz and 19 GHz channels. These two filters are used in this research as follows: SIC for image pixels with GR(37/19) values greater than 0.13 and GR(22/19) values greater than 0.085 are set to zero.

4. Validation

4.1 Validation with SIC of aerial photography during CHINARE-2012

To match the spatial resolution of aerial photography to the footprint size of satellite instruments (25km), for each flight, the satellite-derived ice concentration recorded on the same day as the flight was interpolated to each location of aircraft observation using the value of the closest grid point. The aerial sea ice concentration was smoothed by a moving average to fit to the resolution of satellite data (Lu et al., 2010). The comparison between average value of aerial photography (black line) and HY2/NT (blue line) is plotted on Fig. 2, together with sea ice concentration from SSMIS/NT (green line) and SSMIS/ASI (red line).

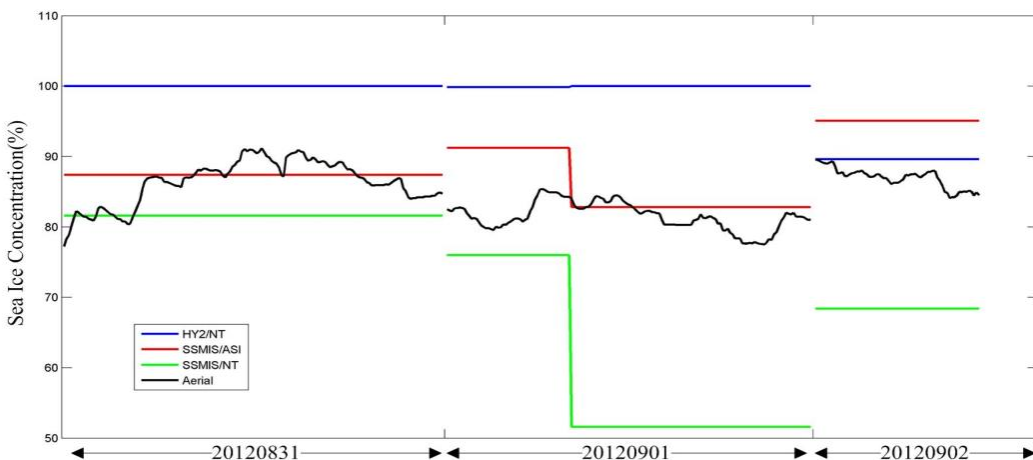


Figure 2. Comparisons of sea ice concentration retrievals between from aerial photography and from satellite remote sensing of HY2/NT, SSMIS/NT, and SSMIS/ASI.

It is interesting from Fig.2 that all satellite remote sensing data overall agree with the in-situ aerial photography at the compact ice regions with ice concentration greater than 80%. However, the HY2/NT data still overestimate the in-situ observations by 16%, while the SSMIS/NT data underestimate the in-situ observations by 17%, only the SSMIS/ASI data give a nice comparison with the aerial photography although a little overestimate of only 4% in satellite data can be found. Such differences are attribute to many factors and difficult to clearly explain. In general, satellite remote sensing is likely to overestimate the in-situ ice conditions at compact ice regions, because the coarse spatial resolution makes it unable to distinguish narrow open leads from large areas of pack ice which is easy to be detected by in-situ aerial photography on the contrary (Hall et al., 2002). Thus the SSMIS/ASI data agree better with the in-situ ice conditions than the HY2/NT data, possibly because it employed the brightness temperature at 89GHz with a spatial resolution of 6.25 km, higher than that for HY2/NT and SSMIS/NT. Such overestimation can be also presumably caused by the recently refrozen, snow-free leads with thin ice covers in the central Arctic. They were classified as water in the aerial observations because of their dark appearance, but their microwave polarization difference is so small that it contributed to an increase in ice concentration retrieved by the ASI or NT algorithm in this footprint (Heygster et al., 2009; Lu et al., 2010).

4.2 Validation with SIC of SAR wind speed images

Higher resolution visible imagery under clear sky, such as MODIS, AVHRR and Landsat, is used to validate the microwave sea ice concentration products in many studies (Cavalieri et al., 2006). SAR image is another data source for the validation. Wiebe et al. (2009) validated the ASI ice concentration with ENVISAT and Radarsat SAR images. The result showed that ASI underestimates the ice concentrations near the ice edge but overestimates them in some interior areas. Anderson et al. (2007) validated seven passive microwave sea ice concentration algorithms with 59 wide swath SAR scenes. Here we selected six images on Nov., 2013 to validate the three products, and the locations of them are defined in Fig.1a. Figure 3a shows one of the images over the Greenland Sea on Nov. 13, 2013. The data were transformed into polar-stereographic grids with a resolution of 500m. After the ice were masked (Fig. 3b) using the thresholding segmentation, the ice concentration from SAR was calculated by averaging the small SAR pixels over the size of the microwave radiometer pixels on the grid of 25 km (Fig. 3c).

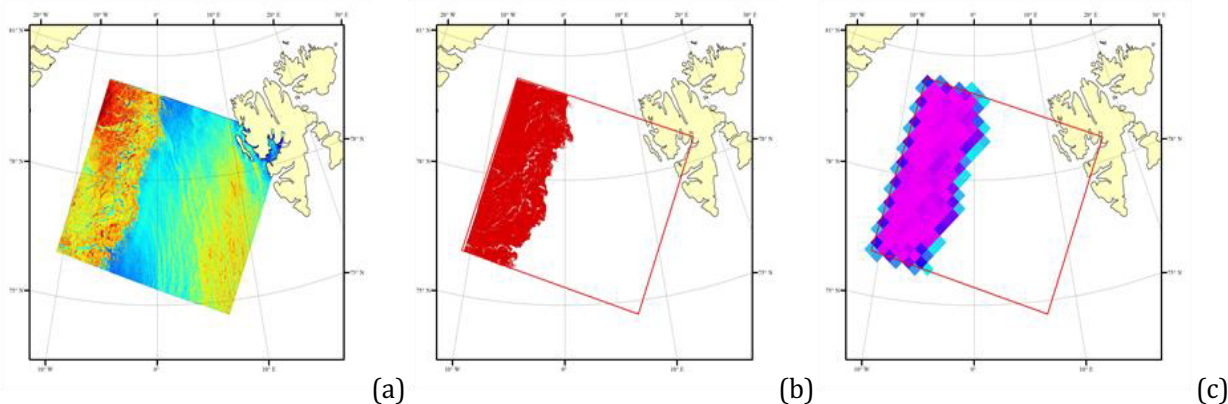


Figure 3. SAR wind speed image (a), segmented ice with a spatial resolution of 500 m (b), and corresponding SIC with a spatial resolution of 25 km (c).

The details of the selected SAR images are summarized in Table 3, and these images cover land and ice edge areas. For the SIC comparison between SAR and radiometer, the data over costal area and open water were excluded. The RMS errors of all SAR images are shown in Table 3. The RMS errors of our result are quite large, ranging from 22.42% to 33.15%. Comparisons with SSMIS/NT and SSMIS/ASI are better and the minimum RMS error is 13.69% and 13.03% respectively. Among the 6 images, the new ice and FYI were distributed in scenes 3, 4 and 6, and the FYI mainly covered the other three. So the results of scene 3, 4 and 6 are worse than that of other three images, which is consistent with previous studies (Wiebe et al., 2009; Xi et al., 2013). The errors of the ice edge areas are higher than that of the interior areas, which is possibly attributed to the time difference between SAR and radiometer observations, thus resulting in substantial changes in SIC over the diffuse marginal ice zones (Wiebe et al., 2009). If the pixels over ice edge areas are removed in the validation, the RMS of three products will significantly decrease below the values in Table 3. For example, the matched pixels number of scene 2 will become 87 and the RMS of HY2/NT, SSMIS/NT and SSMIS/ASI will be 9.64%, 8.59% and 6.17% respectively.

Table 3. Details of the six SAR images and corresponding validation results.

SAR image	Date	Location	Time	Pixels	HY2/NT RMS (%)	SSMIS/NT RMS (%)	SSMIS/ASI RMS (%)
Scene 1	10 Nov.	Greenland Sea	6:52	174	23.96	14.40	13.03
Scene 2	13 Nov.	Greenland Sea	7:05	118	22.42	13.69	16.28
Scene 3	18 Nov.	Kara Sea	2:59	167	33.15	27.83	32.87
Scene 4	21 Nov.	Kara Sea	7:33	158	29.47	34.08	23.55
Scene 5	21 Nov.	Chukchi Sea	18:20	161	23.46	17.02	26.21
Scene 6	23 Nov.	Chukchi Sea	17:21	54	26.24	21.95	25.59

5 Conclusion

The SIC based on brightness temperature data of the HY-2 scanning microwave radiometer is validated using the in-situ aerial photography during CHINARE-2012 and SAR images. Aerial photography conducted during CHINARE-2012 was also employed to produce Arctic sea ice concentration and then compared with the retrieval of satellite remote sensing after spatial interpolation. HY2/NT is 16% higher than the results of aerial photography at the compact ice regions in the central Arctic where the helicopter flights during CHINARE-2012 was carried out. In contrast, the SSMIS/NT data underestimate the in-situ ice concentrations by 17%. While the SSMIS/ASI data show a nice agreement with the result of in-situ photography, possibly because of its higher spatial resolution of 6.25 km than other satellite data. Six SAR images were finally used for the validation of SIC retrievals HY2/NT, SSMIS/NT and SSMIS/ASI. The RMS errors between HY2/NT and SAR, ranging from 22.42% to 33.15%, are larger than that of SSMIS/NT and SSMIS/ASI which are in the range of 13-34% with an average of 22%. The RMS errors in ice edge areas are higher than that of the interior areas. If pixels at ice edges are removed, the RMS between SAR derived ice concentration and three microwave retrievals falls below 10%.

Acknowledgements

This study is part of International Scientific And Technological Cooperation Projects under No. 2011DFA22260, CHINARE2013-02-04 and 2012-04-03-02. We thank all crew on R/V Xuelong for their help on the sea ice observations under the supported of Public Science and Technology Research Funds Projects of Ocean (201205007-05) during CHINARE-2012 which was

organized by the Chinese Arctic and Antarctic Administration. We also thank the NSIDC and University of Bremen for supplying SIC data and NIC for supplying the SAR wind speed images.

References

- Andersen S, Tonboe R, Kaleschke L, et al. 2007. Intercomparison of passive microwave sea ice concentration retrievals over the high-concentration Arctic sea ice. *Journal of Geophysical Research*, 112(C8), doi:10.1029/2006JC003543.
- Cavalieri D J, Crawford J, Drinkwater M R, et al. 1991. Aircraft active and passive microwave validation of sea ice concentration from the DMSP SSM/I. *Journal of Geophysical Research*, 1991, 96(C12), 21989–22009.
- Cavalieri D J, Parkinson C L, Gloersen P, et al. 1996. Updated yearly. Sea Ice Concentrations from Nimbus-7 SMMR and DMSP SSM/I-SSMIS Passive Microwave Data. Boulder, Colorado USA: NASA DAAC at the National Snow and Ice Data Center.
- Cavalieri D J, Markus T, Hall D K, et al. 2006. Assessment of EOS Aqua AMSR-E Arctic sea ice concentrations using Landsat-7 and Airborne microwave imagery. *IEEE Transactions on Geoscience and Remote Sensing*, 44(11), 3057–3069.
- Comiso J C. 1995. SSM/I concentrations using the Bootstrap algorithm. *NASA Reference Publication* 1380, 40 pages.
- Hall R J, Hughes N, Wadhams P. 2002. A systematic method of obtaining ice concentration measurements from ship-based observations. *Cold Regions Science and Technology*, 34(2), 97–102.
- Heygster G, Wiebe H, Spreen G, et al. 2009. AMSR-E geolocation and validation of sea ice concentrations based on 89 GHz data. *Journal of the Remote Sensing Society of Japan*, 29(1), 226–235.
- Inoue J, Curry J A, Maslanik J A. 2008. Application of aerosondes to melt-pond observations over Arctic sea ice. *Journal of Atmospheric and Oceanic Technology*, 25(2), 327–334.
- Lomax A S, Lubin D, Whritner R H. 1955. The potential for interpreting total and multiyear ice concentrations in SSM/I 85.5 GHz imagery. *Remote Sensing of Environment*, 54(1), 13–26.
- Lu Peng, Li Zhijun, Cheng Bin, et al. 2010. Sea ice surface features in Arctic summer 2008: Aerial observations. *Remote Sensing of Environment*, 114(4), 693–699.
- Markus T, Cavalieri D J. 2000. An enhancement of the NASA Team sea ice algorithm. *IEEE Transactions on Geoscience and Remote Sensing*, 38(3), 1387–1398.
- Perovich D K, Tucker III W B, Ligett K A. 2002. Aerial observations of the evolution of ice surface conditions during summer. *Journal of Geophysical Research*, 107(C10), doi:10.1029/2000JC000449.
- Svendsen E, Mtzler C, Grenfell T C. 1987. A model for retrieving total sea ice concentration from a spaceborne dual-polarization passive microwave instrument operating near 90GHz. *International Journal of Remote Sensing*, 8(10), 1479–1487.
- Wiebe H, Heygster G, Markus T. 2009. Comparison of the ASI ice concentration algorithm with Landsat-7 ETM+ and SAR imagery. *IEEE Transactions on Geoscience and Remote Sensing*, 47(9), 3008–3015.
- Xi Ying, Sun Bo, Li Xin. 2013. Assessment of AMSR-E ASI sea ice concentration using ship observations and Landsat-7 ETM+ imagery. *Journal of Remote Sensing*, 17(3), 514–526.